RSC Advances

PAPER

View Article Online
View Journal | View Issue

Cite this: *RSC Adv.*, 2020, **10**, 26319

Fabrication of hierarchically porous superhydrophilic polycaprolactone monolith based on nonsolvent-thermally induced phase separation†

Yu Cao,[a] Wenjuan Han, *[a] Ziyang Pu,[a] Xiaofeng Wang,[b] Bo Wang,[a] Chuntai Liu,[c] Hiroshi Uyama[d] and Changyu Shen[c]

Received 27th May 2020
Accepted 8th July 2020

DOI: 10.1039/d0ra04687f

rsc.li/rsc-advances

Monoliths with a continuous porous structure are of great interest due to high transfer efficiency and large surface area in environmental and tissue engineering fields. This study demonstrated a facile method to prepare PCL monoliths with hierarchically porous structure by nonsolvent-thermally induced phase separation. A suitable mixed solvent mixture using ethanol as nonsolvent reduced the amount of dioxane and provided PCL monoliths with three levels of structures. The monolith structure was easily controlled by changing the fabrication parameters, such as the nonsolvent, the temperature of phase separation, the concentration of the PCL. Finally, the superhydrophilic monolith was easily obtained by polydopamine surface modification. The easy way of fabrication of a hierarchically porous PCL monolith with superhydrophilicity will find applications such as in tissue engineering and purification.

1. Introduction

Hierarchically porous monoliths with macropores (>50 nm) and mesopores (2–50 nm) are generally highly porous, with high surface area, large accessible space, low density and interconnected hierarchical porosity at different length scales.[1] Owing to their diversity and performance, hierarchically porous monolith have been attractive for applications in wastewater treatment, battery electrodes and tissue engineering.[1–6] As a result, the fabrication of hierarchical monoliths with sufficient porosity, tunable pore size and interconnected 3D pores is attracting a lot of attention.

Up to now, many methods have been reported to fabricate hierarchically porous polymeric monoliths, such as porogen leaching, electrospinning, emulsion-templated, foaming and self-assembly.[7–10] Porogen leaching is helped with additives, such as salt and sugars.[11] The electrospinning process fabricates fibers with tunable diameters, however, it is challenged with well-defined 3D porous structures and geometries.[12] The emulsion-templated method usually contains additives because of polymerization from monomer, which is difficult to simultaneously control the polymerization and pore-forming process.[13] The foaming technology requires the precise control on the forming agent and the pore structures simultaneously, which is also by the aid of sophisticated devices.

Phase separation is an effective method to prepare hierarchically porous materials due to the advantages of simple equipment requirement and easy operation, which can be divided by thermally induced phase separation (TIPS) and nonsolvent induced phase separation (NIPS).[5,14–19] In addition, the combined nonsolvent-thermally induced phase separation (NTIPS) method are also applied to fabricate porous monolith by employing a miscible solvent mixture and by controlling the temperature.[20,21] However, the relationship of the fabrication parameters and the desired structures have not been fully elucidated.

Poly(ε-caprolactone) (PCL), biodegradable polymer, is attractive as it has longer degradation time, flexible and tough mechanical properties.[22,23] In the present study, PCL monolith will be fabricated by NTIPS method. The effect of processing parameters, including nonsolvent, phase separation temperature (T_{ps}) and PCL concentration (C_{PCL}), on the morphology of PCL monolith is discussed. Furthermore, the surface hydrophilicity of PCL monolith is adjusted by a one-step method.

[a]School of Materials Science & Engineering, Zhengzhou University, Zhengzhou 450001, China. E-mail: wenjuan.han@zzu.edu.cn

[b]School of Mechanics and Engineering Science, National Center for International Research of Micro-Nano Molding Technology, Key Laboratory of Henan Province for Micro Molding Technology, Zhengzhou 450001, China

[c]Key Laboratory of Materials Processing and Mold, Ministry of Education, National Engineering Research Center for Advanced Polymer Processing Technology, Zhengzhou University, Zhengzhou 450001, China

[d]Department of Applied Chemistry, Graduate School of Engineering, Osaka University, Suita, 565-0871, Japan

† Electronic supplementary information (ESI) available. See DOI: 10.1039/d0ra04687f

2. Experimental

2.1 Materials

PCL was purchased from Swiss Perstorp(CAPA 6500, $M_n = 5 \times 10^4$ g mol^{-1}). Dioxane and ethanol were purchased from Tianjin Fuyu Fine Chemical. Dopamine hydrochloride was purchased from Beijing Huawei Ruike Chemical. Tris was purchased from Haiyuan Ye Biotechnology. Deionized water was used as provided.

2.2 Preparation of PCL monolith

Fig. 1 showed schematic of PCL monolith preparation process. Firstly, a certain amount of PCL and solvent mixture were mixed in a glass tube by heating at 55 °C with mechanical agitation for 4 hours to get a transparent uniform solution. After that, the glass tube was placed at different temperatures for phase separation for 24 hours to get wet PCL monolith. Finally, wet PCL monolith was washed in deionized water and dried in lyophilizer. The preparation parameters are listed in Table 1. In this study three T_{ps} were chosen, 20 °C, 4 °C, −18 °C, which were room temperature, refrigerated temperature and freezing temperature, respectively. The other preparation parameters were decided by the phase diagram which was determined by the calculated of cloud point, as shown in Fig. S1 and S2.†

2.3 Surface modification of PCL monolith

0.1 g of dopamine hydrochloride was dissolved in the mixture of 50 mL Tris–HCl buffer (pH = 8.5) and 20 mL ethanol. The solution was stirred until the solution changed from colorless to dark black to form polydopamine (PDA). Then, the PCL monolith (sample-4 obtained in Saection 2.2) was immersed in the as-prepared PDA solution with degassing for 18 hours. After that the monolith was washed with deionized water and subsequently dried at 40 °C for 12 hours in a vacuum oven to obtain the PDA-PCL monolith.

2.4 Characterization

Surface morphologies of the samples were observed with a field emission scanning electron microscope (SEM, Hitachi S3000N). A thin gold film was sputtered on the samples before the images were collected. N_2 adsorption/desorption isotherms were measured with a NOVA 4200e Surface Area & Pore Size Analyzer (Quantachrome Instruments) at 77 K. Before the measurements, all samples were degassed at 20 °C under vacuum for at least 6 hours. The Brunauer–Emmett–Teller (BET) method was utilized to determine the specific surface areas and Density Functional Theory (DFT) method was applied to calculate the pore sizes distribution. Differential scanning calorimetry (DSC) thermograms was taken using a Seiko DSC6020 instrument at the heating/cooling rate of 10 °C min^{-1} under nitrogen. Water contact angles (CA) were measured on a contact angle analysis system (Zhongchen JC2000C) at room temperature with 5 μL of water droplets as indicators. The surface chemistry of the membranes was characterized by a Fourier transform infrared spectrometer (FT-IR, NICOLET IS50). The transmittance of each sample was recorded between 4000 cm^{-1} and 500 cm^{-1} with a resolution of 2 cm^{-1}. The PDA coating on the surface of PCL monolith was analyzed by X-ray photoelectron spectroscopy (XPS, Miniscope TM 3000 equipped with Swift ED 3000 Hitachi). The XPS N 1s core-level signal was used as a marker for the analysis of the PDA on the surface.

Table 1 The parameter conditions of preparing the PCL monolith

Sample	C_{PCL} (mg mL^{-1})	Solvent mixture dioxane/ethanol (v/v)	T_{ps} (°C)
1	80	30/70	−18
2	80	30/70	4
3	80	30/70	20
4	100	30/70	20
5	120	30/70	20
6	140	30/70	20
7	140	25/75	20

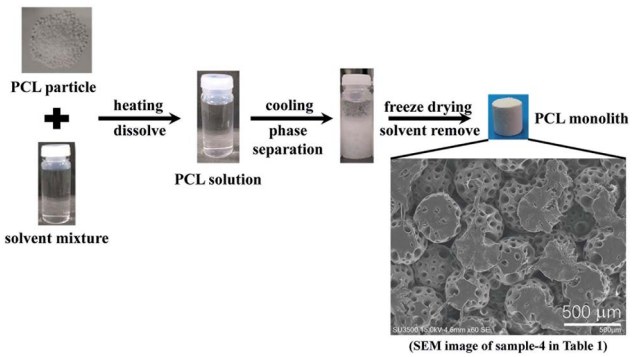

Fig. 1 Schematic of fabricating PCL monolith *via* phase separation.

3. Results and discussion

3.1 The Hansen solubility parameters

In this study, the dioxane was employed as the good solvent for PCL dissolving. The ethanol was selected as nonsolvent to induce the NTIPS due to its environmentally friendly, low toxicity and low cost. When the solvent mixture of dioxane and ethanol at the volume ratios of 25/75, 30/70 (recorded as E25/75, E30/70), respectively, the PCL monolith could be obtained at the T_{ps} of 20 °C, 4 °C and −18 °C. At the phase separation temperature, the solvent mixture of E30/70 was still liquid, as shown in Fig. S3.†

To investigate the interaction of PCL and the solvents, the distance D between the solvent and the solute in the "solubility space" which affected the solubility of polymers in solvents was calculated based on the Hansen's solubility theory. According to the referenced formulae (S1)–(S3),† the solubility parameters of different materials were calculated and listed in Table S2.†

In general, when the distance D between the solvent and the polymer was less than 7.5, the solvent was regarded as a good solvent, otherwise the solvent was a nonsolvent.[24,25] The distance D between the polymer and different solvent at different T_{ps} was shown in Fig. 2. It can be found that the D

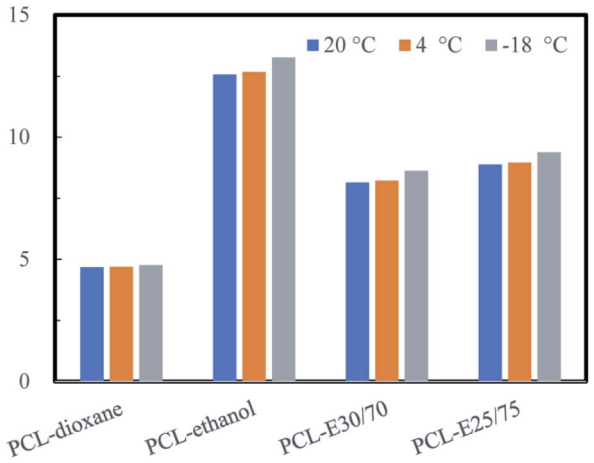

Fig. 2 The distance D between the polymer and different solvent at different T_{ps} (20 °C, 4 °C, −18 °C respectively).

between PCL and solvent mixture (E25/75 and E30/70) were all higher than 7.5, which explained the reason that phase separation can easily be generated at all three temperatures, and the monoliths were obtained accordingly.

The experimental and theoretical results suggested that the ethanol was an efficient nonsolvent, because the phase separation could take place even at room temperature which was higher than the freezing point of the solution. Therefore, the ethanol acting as nonsolvent in this study enlarged the processing window and reduced the energy consumption in the preparation of PCL monolith. In addition, the distance D, the Hanses solubility parameter, can provide an effective way to predict whether phase separation could occur in different solution systems.

3.2 Morphology control of the PCL monolith

Phase separation method had been extensively applied in fabrication of monolith. In a TIPS process, the presence of temperature gradient induced spatial variation leading to a change in chemical potential, which was the driving force for phase separation. When the thermodynamic equilibrium was broken, liquid–liquid phase separation in a polymer-rich and a polymer-lean phase can take place, which includes two phase separation mechanism namely nucleation growth (NG) mechanism and spinodal decomposition (SD) mechanism.[26] The polymer-rich phase leaded the skeleton and the polymer-lean phase leaded the pores. By introducing a nonsolvent in this NTIPS method, ethanol, the increased potential of polymer precipitation further promoted the efficiency of TIPS. The effect of fabrication parameters on the morphology of the PCL monolith based on the NTIPS method was discussed.

3.2.1 The ethanol ratio. The effect of ethanol ratio in the solvent mixture on the morphology was studied. Fig. 3 showed the porous structure at solvent mixture of E30/70 and E25/75, respectively (T_{ps} at 20 °C, C_{PCL} of 140 mg mL^{-1}). It was interesting to see that a PCL monolith was composed of stacking golf-like structure with a lot of pores on the surface. With the ethanol concentration increased from 70% to 75%, the average

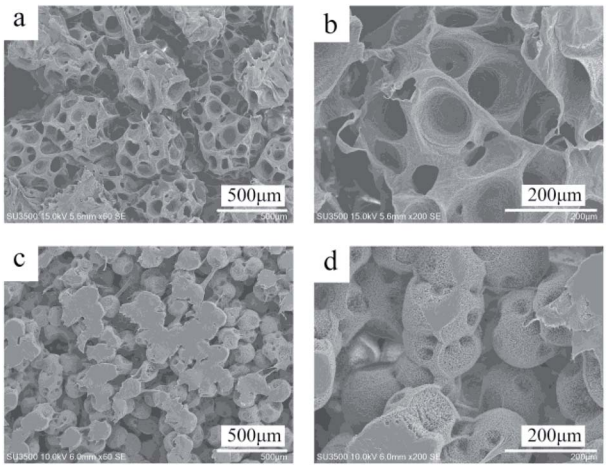

Fig. 3 SEM of the morphology of PCL monolith at different ethanol ratios, 75% (a and b), 70% (c and d) respectively. (b and d) Are enlarged images of a specific area from (a and c), respectively. (T_{ps} at 20 °C, C_{PCL} of 140 mg mL^{-1}).

diameter of the sphere increased from 155 μm to 478 μm. The density of round pore on the sphere became higher and the size became larger, from 36 μm to 114 μm. Pore size would affect the performance of monolith such as the compressive properties (Fig. S6†). In addition, the surface of the sphere in Fig. 3(d) was not smooth but was "lotus-leaf-like" with even smaller features. However, the roughness of the surface of sphere in Fig. 3(b) decreased significantly. It can be seen in Fig. 2 that the

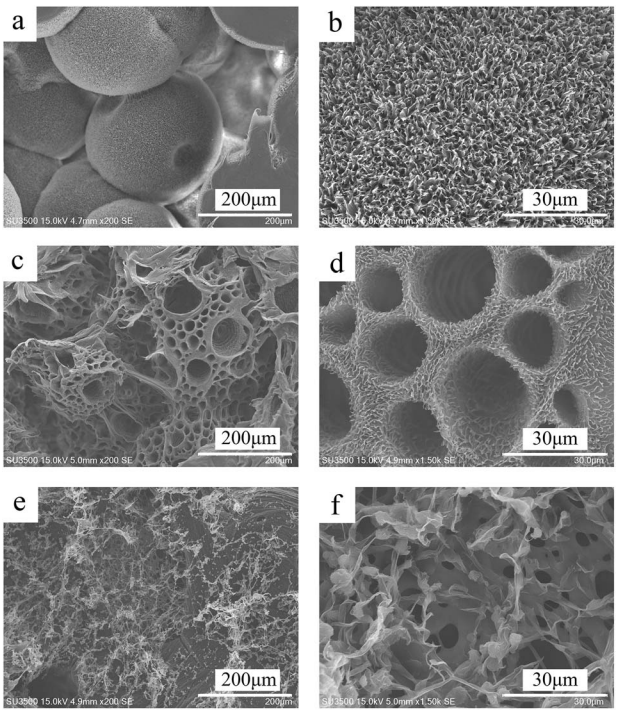

Fig. 4 SEM of the morphology of PCL monolith at different T_{ps} of 20 °C (a and b), 4 °C (c and d) and −18 °C (e and f). (b and d) Are enlarged images of a specific area from (a and c), respectively. (E30/70, C_{PCL} of 80 mg mL^{-1}).

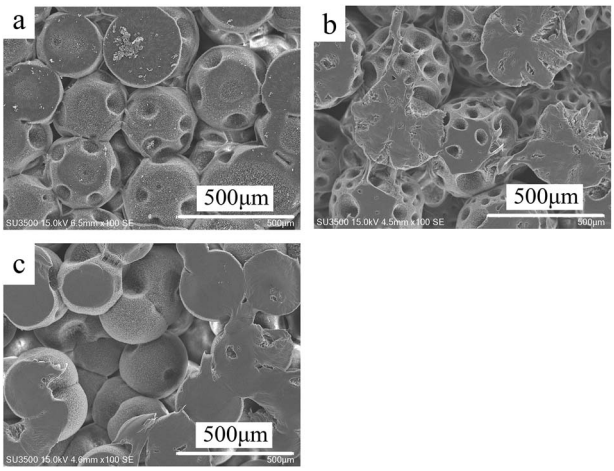

Fig. 5 SEM of the morphology of PCL monolith at different PCL concentrations, 120 mg mL^{-1} (a), 100 mg mL^{-1} (b), 80 mg mL^{-1} (c). (E30/70, T_{ps} at 20 °C).

solubility of PCL in the solvent with 75% ethanol was lower than that with 70% ethanol. Therefore, the solubility might play a key role in the formation of the porous structure.

The globular structure might be the result of the NG mechanism in the liquid–liquid (L–L) phase separation, and subsequently a crystallization process taking place in the polymer rich phase. During the crystallization, crystal lamellae grew freely in 3D space from the center, showing spherulite shapes. It was known that crystallization in solution followed the similar rules within polymer melt when the solution concentration was high (not dilute solution), namely nucleation and growth. Firstly, there should be nuclei formed by either self-assembly (homogeneous nucleation) or as-existed impurities (heterogeneous nucleation). The molecular chains diffused and arranged themselves in a crystal lattice and thus the crystallite grew to be larger and larger. In the solvent mixture, the solvent and non-solvent served as impurities. When more nonsolvent was added in the solution, the dissolvability of PCL decreased, therefore the interaction between polymer and solvent became weaker. Furthermore the viscosity of the solution system decreased accordingly, then polymer chains can more easily arrange to the sphere particles.[27] As a result, the sphere particle showed a larger diameter in E25/75 than that in E30/70. The pores shown on the surface of sphere might be the result of aggregated solvent molecules due to the repulsion of freeze drying.[28]

3.2.2 The phase separation temperature. Fig. 4 showed the morphology of PCL monoliths at different T_{ps} of 20 °C, 4 °Cand −18 °C, respectively. As mentioned above, the PCL monolith with golf-like sphere and "lotus-leaf-like" surface was obtained at the temperature of 20 °C. A higher magnification images showed that the rough surface of the sphere was composed of porous structure from a smaller scale of which formed by tiny lamellae connected with each other. As the T_{ps} decreased down to 4 °C, honeycomb-like continuous structures were obtained which were composed of skeleton and pores, while the sphere was not easily observed. There were tiny lamellae shown on the

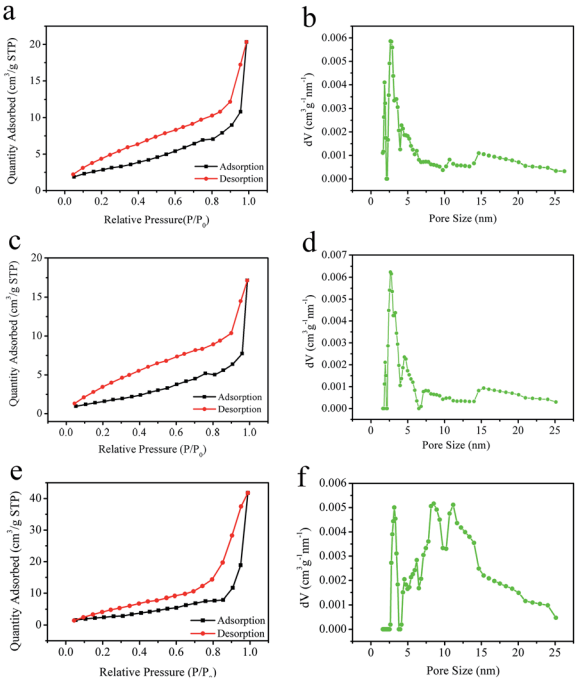

Fig. 6 BET results of PCL monoliths fabricated by different T_{ps} were 20 °C (a and b); 4 °C (c and d); −18 °C (e and f), respectively. (a, c and e) are nitrogen adsorption/desorption isotherms, (b, d and f) are the pore size distribution plots. The concentration is of 100 mg mL^{-1} with the solvent of E30/70.

skeleton and the round pores with the average diameter of about 30 μm when the temperature was 4 °C. The density was also decreased from 0.20 g cm^{-3} to 0.18 g cm^{-3}, which was shown in Fig. S5.† As the temperature decreased to −18 °C, bicontinuous structures was formed *via* SD. The reason is that homogeneous polymer solution can entry directly from one-phase state to two-phase state during phase separation with high cooling rate.[26] However, fibrous structure at some site can also be clearly seen. Interestingly, the surface roughness of the porous structure becomes smaller when the T_{ps} decreases from 20 °C, 4 °C to −18 °C. The dramatical differences in the microstructure might suggest that the phase separation mechanisms behind are different from each other with the temperature variation.

The relationship between the structural feature and T_{ps} reveals that the phase separation temperature played a dominant role on the morphology of PCL monoliths. When the T_{ps} was 20 °C, the phase separation was regarded as the NG mechanism in the L–L phase separation. And a slow cooling rate leaded to a fast crystal growth rate and formation of large "lotus-leaf-like" crystal lamellae. As the temperature decreased to 4 °C, the phase separation changed to NG mechanism of the L–L phase separation. And the PCL solution showed a higher nucleation rate and a lower crystal growth rate, which resulted that the crystal lamellae seemed smaller. When the T_{ps} was −18 °C,with a SD mechanism, the instant nucleation and very slow crystal growth resulted in the formation of fibrous structure.[29]

Table 2 DSC result of PCL particle and monolith

Sample	χ_c (%)	T_m (°C)
PCL particle	55	59
PCL monolith-20 °C	74	61
PCL monolith-4 °C	82	61
PCL monolith-18 °C	60	63

3.2.3 The PCL concentration. Fig. 5 showed the morphologies of the monoliths at different PCL concentrations of 120 mg mL^{-1}, 100 mg mL^{-1} and 80 mg mL^{-1}. The porous structure was all packed spherical structure with small round pores. The average diameter of the spherical structure composed with stacked crystal lamellar increases from 155 μm to 497 μm with the decrease of the C_{PCL} from 140 mg mL^{-1} to 100 mg mL^{-1} and then decreased to 254 μm at the C_{PCL} of 80 mg mL^{-1}. Furthermore, when two spherulites grew to contact with each other, the growth of the spherulites was limited and the contact surface of the two spherulites became flat.

As the concentration of the PCL solution decreased, the viscosity of the PCL solution decreased accordingly. And it was easier for the PCL molecular chain to rearrange to crystalize, which resulted in a larger diameter of the stacking golf-like structure at 20 °C. However, as the C_{PCL} became to 80 mg mL^{-1}, the diameter of the balls decreased due to the number of rearranged crystal chains decreased. This result suggested that the temperature regulate the phase separation mechanism, while solution concentration might affect the geometric dimension of a specific porous feature.

3.3 The hierarchical structure of PCL monolith

Fig. 6(a), (c) and (e) shows the adsorption/desorption isotherms of the PCL monolith at 77 K, which was a type V adsorption with H1 type hysteresis loop in the P/P_0 range from 0.2 to 1.0, whose characteristic was mesoporosity and low energy of adsorption. The specific surface area was determined to be 10.4 m^2 g^{-1}, 6.5 m^2 g^{-1}, 9.1 m^2 g^{-1} for the samples at the T_{ps} of 20 °C, 4 °C, to −18 °C, considering monolayer adsorption by using BET method. These valuescan be compared to the PCL nanofibers with the specific surface area about 7.3 m^2 g^{-1} (average diameter 160 nm), indicating that the PCL monolith had a relatively large specific surface area.[30] Fig. 6(b), (d) and (f) display the pore size distribution using the DFT method, which showed that the diameters of the uniform pores were 5.5 nm, 5.3 nm, 9.3 nm, respectively. The results suggested there were numerous nanopores in the monoliths obtained at different T_{ps}, which might contribute significantly to the specific surface area of the monolith. Furthermore, these data indicated that the formation of hierarchically porous structures with relatively uniform mesopores in the PCL monolith.

3.4 Crystallization of the PCL monolith

Fig. S4† showed the DSC curves of the first heating of the PCL particle and the PCL monoliths fabricated at different T_{ps}. The calculated DSC result was shown as Table 2. The degree of crystallinity of all the PCL monolith was higher than that of PCL

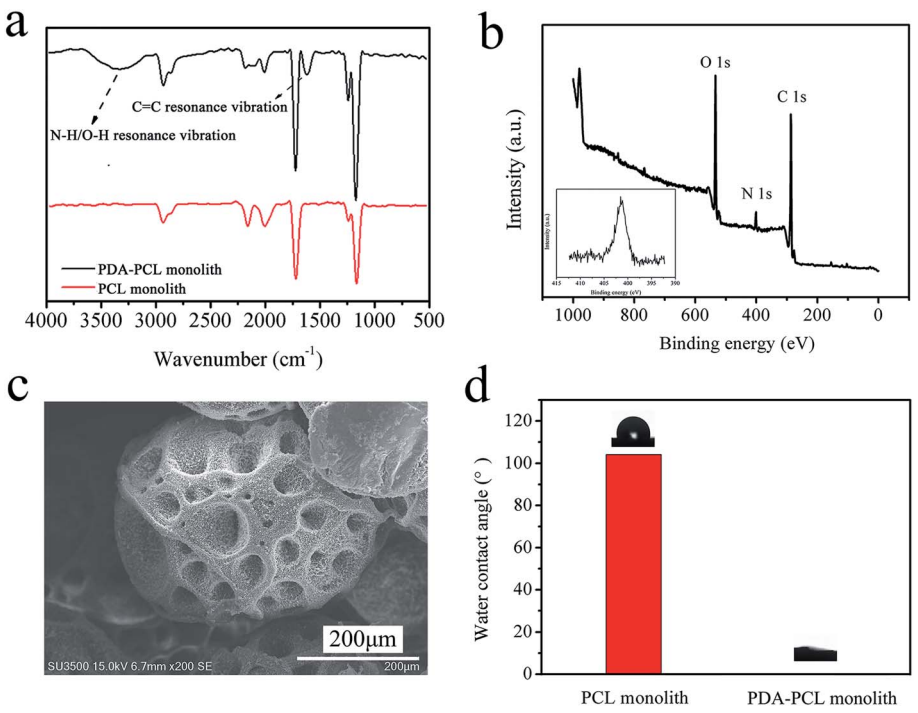

Fig. 7 (a) FT-IR spectra of PCL and PDA-PCL monolith (b) A wide scan XPS spectra and enlarged N1s XPS spectra (inside) of PDA-PCL monolith (c) SEM of PDA-PCL monolith (d) water contact angle of PCL and PDA-PCL monolith.

particles at 55%, which was also much higher than that of PCL foams at 37% reported.[23] The PCL monolith obtained at 4 °C had the highest degree of crystallinity, 82%. While the melting temperature was all around 61 ± 2 °C, suggesting that the crystalline structure was almost the same. The high degree of crystallinity result indicated that the as-mentioned rough surface of the globular structure was the PCL crystal lamellae.

3.5 Characterization of modified PDA-PCL monolith

In order to investigate the surface composition after modification, chemical characteristics of PCL and PDA-PCL monolith surface was tested by ATR-FTIR spectroscopy. As shown in Fig. 7(a), the new peaks at 3600–3100 cm^{-1} and 1600 cm^{-1} appeared in the spectrum of PDA-PCL monolith, which were due to the stretching vibration of the –NH and –OH groups and the resonance movement of the C=C bond on the benzene ring from PDA.[31] The PDA-PCL monolith was further confirmed by XPS measurements. Fig. 7(b) showed an XPS wide scanning and N 1s core-level spectra of the PDA-PCL monolith respectively. The N 1s core-level spectrum of the PDA-PCL monolith had one peak component with the binding energy at about 400 eV, due to the PDA on the monolith surface.[31] The morphology of PDA-PCL monolith was shown in Fig. 7(c). It can be clearly observed that there were plenty of tiny white dots attached on the rough surfaces homogeneously. Compared to the neat PCL monolith, the contact angle of PDA-PCL sharply decreased from 105° to nearly 0, and water uptake increased from 74% to 80%, which revealed that a superhydrophilic PDA-PCL monolith was obtained (Fig. 7(d) and S7†).

The hydrophobicity of PCL porous materials hindered the further applications in tissue engineering and other fields.[32–34] As a result, the surface chemistry using adhesive catecholamine inspired by mussel adhesion was developed, which was based on the easy self-polymerization of dopamine to form PDA with the adhesive-layer on any materials.[35] The PDA coating was achieved by combined pathways of non-covalent self-assembly of dopamine and 5,6-dihydroxyindole and polymerization of the indole, resulting in the formation of a robust layer of PDA.[35] The PDA adhesive-layer might serve as a platform for post-modification. The successful modified PCL monolith by PDA was proved by the result of FT-IR and XPS. And the static water contact angle showed the superhydrophlic of the PDA-PCL monolith. This simple one-step deposition modification of PCL monolith may expand considerably in the range of application in water treatment and tissue engineering.

4. Conclusions

A hierarchically porous PCL monolith was successfully fabricated from a PCL solution by the combination of TIPS and NIPS. A high efficient solvent mixture with ethanol acting as non-solvent provided the PCL monolith with a 3D continuous hierarchically porous structure at different T_{ps}. The result showed that NIPS increased the efficiency of TIPS of PCL solution. The hierarchical structure of the PCL monolith was significantly affected by the phase separation parameters including types of nonsolvent, ratio of solvent/nonsolvent, the C_{PCL} and the T_{ps}. Furthermore, the superhydrophilic PDA-PCL monolith was successfully obtained by PDA modification with one-step deposition method. This method of fabricating the superhydrophilic PDA-PCL monolith provided a more eco-friendly and facile technique with hierarchical porous structure, which might show a great potential in the application of tissue engineering and regenerative medicine.

Conflicts of interest

There are no conflicts to declare.

Acknowledgements

The authors acknowledge financial support from the Key Science &Technology Project for Institutions of Higher Education of Henan Province (No. 19B430010), Key R & D and Promotion Projects in Henan Province, the China 111 Project (D18023) and the Introducing Overseas Intelligence of Henan Province (CXJD2018003, HNGD2020011).

References

1 M. Sun, S. Huang, L. Chen, Y. Li and X. Yang, *Chem. Soc. Rev.*, 2016, **45**, 3479–3563.
2 Y. Liu, D. Luo and T. Wang, *Small*, 2016, **12**, 4611–4632.
3 Z. Chen, *et al.*, *J. Membr. Sci.*, 2020, **603**, 118041.
4 S. D. Lacey, *et al.*, *Adv. Mater.*, 2018, **30**, 1705651.
5 Y. Xin, *et al.*, *Carbohydr. Polym.*, 2017, **157**, 429–437.
6 S. A. Saba, M. P. Mousavi, P. Bühlmann and M. A. Hillmyer, *J. Am. Chem. Soc.*, 2015, **137**, 8896–8899.
7 X. Guo, *et al.*, *Biomacromolecules*, 2020, **21**, 1202–1213.
8 T. Xu, J. M. Miszuk, Y. Zhao, H. Sun and H. Fong, *Adv. Healthcare Mater.*, 2015, **4**, 2238–2246.
9 L. Alison, *et al.*, *Sci. Rep.*, 2019, **9**, 1–9.
10 H. Mi, *et al.*, *ACS Appl. Mater. Interfaces*, 2019, **11**, 7479–7487.
11 L. Zhu, D. Luo and Y. Liu, *Int. J. Oral Sci.*, 2020, **12**, 1–15.
12 L. A. Smith, X. Liu and P. X. Ma, *Soft Matter*, 2008, **4**, 2144–2149.
13 S. M. Silverstein, *Prog. Polym. Sci.*, 2014, **39**, 199–234.
14 A. Elhaj and K. Irgum, *ACS Appl. Mater. Interfaces*, 2014, **6**, 15653–15666.
15 Y. Wang, *et al.*, *J. Hazard. Mater.*, 2018, **344**, 849–856.
16 Q. Bai, Q. Xiong, C. Li, Y. Shen and H. Uyama, *Cellulose*, 2017, **24**, 4275–4289.
17 A. Dobashi, J. Maruyama, Y. Shen, M. Nandi and H. Uyama, *Carbohydr. Polym.*, 2018, **200**, 381–390.
18 K. Okada, *et al.*, *Chem. Commun.*, 2011, **47**, 7422–7424.
19 G. R. Guillen, Y. Pan, M. Li and E. M. Hoek, *Ind. Eng. Chem. Res.*, 2011, **50**, 3798–3817.
20 T. Jin, Z. Zhao and K. Chen, *J. Appl. Polym. Sci.*, 2016, **133**, 42953.
21 H. Matsuyama, Y. Takida, T. Maki and M. Teramoto, *Polymer*, 2002, **43**, 5243–5248.
22 A. H. Ardekani-Zadeh and S. F. Hosseini, *Carbohydr. Polym.*, 2019, **223**, 115108.

23 O. C. Onder, E. Yilgor and I. Yilgor, *Polymer*, 2018, **136**, 166–178.
24 C. M. Hansen, *Hansen solubility parameters: a user's handbook*, CRC press, 2007.
25 C. Bordes, *et al.*, *Int. J. Pharm.*, 2010, **383**, 236–243.
26 P. V. D. Witte, P. J. Dijkstra, J. W. A. V. D. Berg and J. Feijen, *J. Membr. Sci.*, 1996, **117**, 1–31.
27 T. Alfrey, A. Bartovics and H. Mark, *J. Am. Chem. Soc.*, 1942, **64**, 1557–1560.
28 S. Liu, Z. He, G. Xu and X. Xiao, *Mater. Sci. Eng., C*, 2014, **44**, 201–208.
29 J. Zhao, *et al.*, *Carbohydr. Polym.*, 2011, **83**, 1541–1546.
30 M. Thommes, *et al.*, *Pure Appl. Chem.*, 2015, **87**, 1051–1069.
31 Q. Tu, *et al.*, *Colloids Surf., B*, 2013, **102**, 361–370.
32 D. Mondal, M. Griffith and S. S. Venkatraman, *Int. J. Polym. Mater. Polym. Biomater.*, 2016, **65**, 255–265.
33 M. Mirhosseini, V. Haddadi-Asl and S. S. Zargarian, *J. Appl. Polym. Sci.*, 2016, **133**, 43345.
34 A. Gloria, *et al.*, *Biomacromolecules*, 2012, **13**, 3510–3521.
35 H. Lee, S. M. Dellatore, W. M. Miller and P. B. Messersmith, *Science*, 2007, **318**, 426–430.